Validation of a Computationally Efficient Model of the Mu-Opioid Receptor

Allison Barkdull[a], Lexin Chen[b], Akash Mathavan[c], Karina Martinez-Mayorga[d,e], & Coray M. Colina[b,e,f]*

[a]Department of Biomedical Engineering, University of Florida, Gainesville, FL
[b]Department of Chemistry, University of Florida, Gainesville, FL
[c]College of Medicine, University of Florida, Gainesville, FL
[d]Instituto de Química, Unidad Mérida, Universidad Nacional Autónoma de México, Ucú, Yucatán, México
[e] UAEY-IIMAS, Universidad Nacional Autónoma de México, Mérida, Yucatán, México
[f]Departments of Materials Science and Nuclear Engineering, University of Florida, Gainesville, FL

https://doi.org/10.33697/ajur.2023.085

Students: allisonbarkdull@ufl.edu, le.chen@ufl.edu, amathavan2496@ufl.edu
*Mentors: kmtzm@unam.mx, colina@chem.ufl.edu**

ABSTRACT
The mu-opioid receptor (MOR) is a transmembrane protein and the primary target for pain-modulating drugs. Opioid drugs come with detrimental side-effects such as physical dependence and addiction. However, recent studies show that understanding structural properties and dynamics of MOR may aid in the design of opioid drugs with reduced side effects. Molecular dynamics simulations allow researchers to study changes in protein conformation at an atomistic level. However, modeling systems including MOR embedded in a lipid bilayer can be computationally expensive. This study evaluates a modeling approach that uses harmonic restraints on the transmembrane regions of MOR to model the rigidity of the lipid bilayer without explicitly simulating lipid molecules, reducing the number of atoms in the simulation. The proposed model allows MOR to be simulated 49% faster than a simulation explicitly including the lipid bilayer. To assess the accuracy of the proposed model, simulations were performed of MOR in a lipid bilayer, the free MOR in water and MOR in water with harmonic restraints applied to all transmembrane residues using NAMD 3.0 alpha and the CHARMM36 force field. Dynamic properties of MOR were shown to be different in each system, with the free MOR having a higher root mean square deviation (RMSD) than MOR with an explicitly modeled lipid bilayer. The systems with harmonic restraint constants of 0.001 kcal/mol/Å^2 applied to the transmembrane residues had RMSD values comparable to those in an explicitly modeled lipid bilayer. This study demonstrates that using restraints on the transmembrane residues of MOR is a feasible way of modeling the ligand-free receptor with reduced computational costs. This model could allow the dynamics of MOR in a lipid bilayer environment to be studied more efficiently.

KEYWORDS
Molecular Dynamics; Atomistic Simulations; Computational Modeling; Mu-Opioid Receptor; G-Protein Coupled Receptor; Lipid Bilayer; Opioid; Transmembrane Protein

INTRODUCTION

Opioid receptors are a primary target for analgesic drugs. In 2020, there were 43.3 opiate prescriptions per 100 people in the United States.[1] However, opiates produce adverse side effects such as constipation, nausea, and respiratory depression, and long-term use of opioid drugs can lead to tolerance, physical dependence, and addiction.[2] The widespread abuse of opioid drugs is a major public health crisis which caused 50,178 deaths in the United States in 2019 alone[3]. Because of the limitations of existing opioid drugs, it is necessary to further explore how the opioid receptors can be modulated to minimize undesired effects.

Most pain-killing effects of opioid drugs are attributed to interactions with the mu-opioid receptor (MOR).[4] MOR, depicted in **Figure 1**, is a G protein-coupled receptor (GPCR) which is distributed through the nervous system and digestive tract. Like other GPCRs, MOR has seven transmembrane helices, an extracellular N-terminus and an intracellular C-terminus which can be phosphorylated upon agonist binding.[5] MOR has an orthosteric ligand-binding pocket, highlighted in purple in **Figure 1,** where both agonist and antagonist ligands bind. An agonist is a molecule which binds to a receptor causing a functional activation leading to a signaling cascade within the cell. In the case of MOR, an agonist binding is associated with activation of downstream signaling cascades that lead to a pain-killing effect. Conversely, an antagonist binds to the receptor blocking all other molecules from binding to the orthosteric site and locking the receptor in the inactive state. Upon activation of MOR by an agonist, there is a large outward movement of transmembrane helix 6 and a smaller inward movement of transmembrane helices 5 and 7.[6]

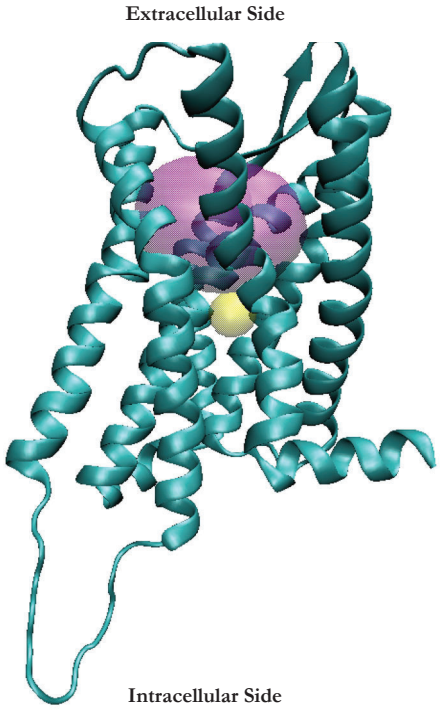

Figure 1. The mu-opioid receptor (PDB ID: 4DKL[22]) shown in blue with the agonist binding site represented in purple and the allosteric sodium binding site in yellow.

Evidence suggests that interactions with different agonists can cause significantly different conformational changes in MOR, leading to preferential activation of different downstream pathways.[7] This process is called functional selectivity or biased agonism.[7] MOR's analgesic effects are attributed to its interactions with heterotrimeric G-proteins[8] which act by inhibiting adenyl cyclase, modulating ion channels, and causing second messenger cascades.[9] However, after activation, MOR can be phosphorylated, leading to β-arrestin binding, which causes receptor desensitization and internalization which may be associated with negative side effects such as tolerance. It has been shown that different agonists cause different levels of G_i coupling and β-arrestin recruitment;[10] however, the exact conformational changes in MOR which lead to these different effects are not fully understood.[7] Finding ligands that can modulate pain with diminished unwanted downstream effects requires a better understanding of the structural changes of MOR when bound to different ligands.

MOR also has an allosteric binding site, highlighted in yellow on **Figure 1**, which plays an important role in the receptor conformation and downstream effects. This binding site is conserved among Class A GPCRs and may hold a sodium ion.[11] The presence of a sodium ion in the allosteric binding site helps stabilize MOR in its inactive state.[12] Site-directed mutagenesis studies replacing the residues which make up the binding site showed that there was significantly increased β-arrestin recruitment when sodium is not present[10] Additionally, computational studies suggest that herkinorin, an opioid which does not promote β-arrestin recruitment or receptor internalization may interact with the allosteric sodium binding site, modulating it.[13,14]

Molecular dynamics simulations are a powerful tool to study MOR dynamics and drug binding at an atomistic level. Molecular dynamics simulations have been used to gain understanding about agonist[15] and antagonist[16] binding properties, the role of the allosteric sodium ion[13,17] and functional selectivity.[18] In other studies, restraints on specific regions of integral membrane proteins have been used to represent features such as ion bridges[19] or to resolve the packing of transmembrane alpha helices in low-resolution crystal structures.[20] However, it can be challenging to study binding mechanisms of ligands to GPCRs such as MOR using all-atom molecular dynamics simulations due to the long time scales necessary to sample conformational states of GPCRs.[21]

This study seeks to evaluate a model of the ligand-free MOR which can be used to study its overall dynamic properties while eliminating the computational cost of explicitly modeling the lipid bilayer. The inactive MOR is simulated both with and without the allosteric sodium ion present in three conditions: the protein in an explicit lipid bilayer, the free protein surrounded by water, and the protein surrounded by water with a harmonic restraint applied to the backbone atoms of the transmembrane residues. Comparisons between the free protein and membrane-protein system allow for the evaluation of the impact of the membrane on protein dynamics. In order to evaluate the accuracy of the restrained protein model, comparisons are made with simulations of MOR in a membrane made of 1-palmitoyl-2-oleoyl phosphatidylcholine (POPC) and 10% cholesterol.

METHODS AND PROCEDURES

Figure 2 shows a summary of the simulation setups. The structure of the inactive mouse MOR was downloaded from the Protein Databank, with PDB ID: 4DKL.[22] In the original crystal structure, in the inactive state, the third intracellular loop was replaced with a T4 lysozyme. The sequence of the third loop is identical to that in the active mouse MOR structure (PDB ID: 5C1M[23]), so the structures were aligned and the residues from the active structure were added to the inactive structure, replacing the T4 lysozyme. While there are some differences between the mouse and human MOR, the amino acid sequences of the two proteins have a 96.2% similarity.[24, 25, 26] Then, the structure was minimized for 1000 steps to reach a more energetically favorable conformation. Each amino acid in the protein was modeled in the protonation state appropriate for a pH of 7.

The membrane-protein system was created by placing the protein in a membrane made of 1-palmitoyl-2-oleoyl phosphatidylcholine (POPC) and 10% cholesterol using the CHARMM-GUI Membrane Builder.[27] The system was buffered by 22.5 Å of cTIP3P[28] water on the top and bottom of the membrane (**Figure 2**, Panels A-B). The free protein system was solvated with cTIP3P[29] water molecules in a 111×111×111 $Å^3$ cubic box to prevent interactions with periodic images (**Figure 2**, C-D).

The restrained protein system was solvated in an orthorhombic box with a 16 Å cTIP3P water buffer on each side of the protein, and the transmembrane residues identified from the PDB entry were restrained during production with varying forces.[22] Five simulations were performed with restraint forces of 20 kcal/mol/Å^2, 5 kcal/mol/Å^2, 1 kcal/mol/Å^2, 0.01 kcal/mol/Å^2, and 0.001 kcal×mol^{-1}×Å^{-2} (**Figure 2**, Panel E-F) on the transmembrane atoms. The free protein system was created by solvating the protein in a 111Å × 111Å × 111Å cubic box of cTIP3P water with no restraints added during the production simulation.

In the restrained protein system, the receptor is held by the restraints in the center of the box and translates less than the free protein system, so a smaller water buffer can be used without the protein interacting with its own periodic images. This smaller water buffer contributes to a higher simulation speed.

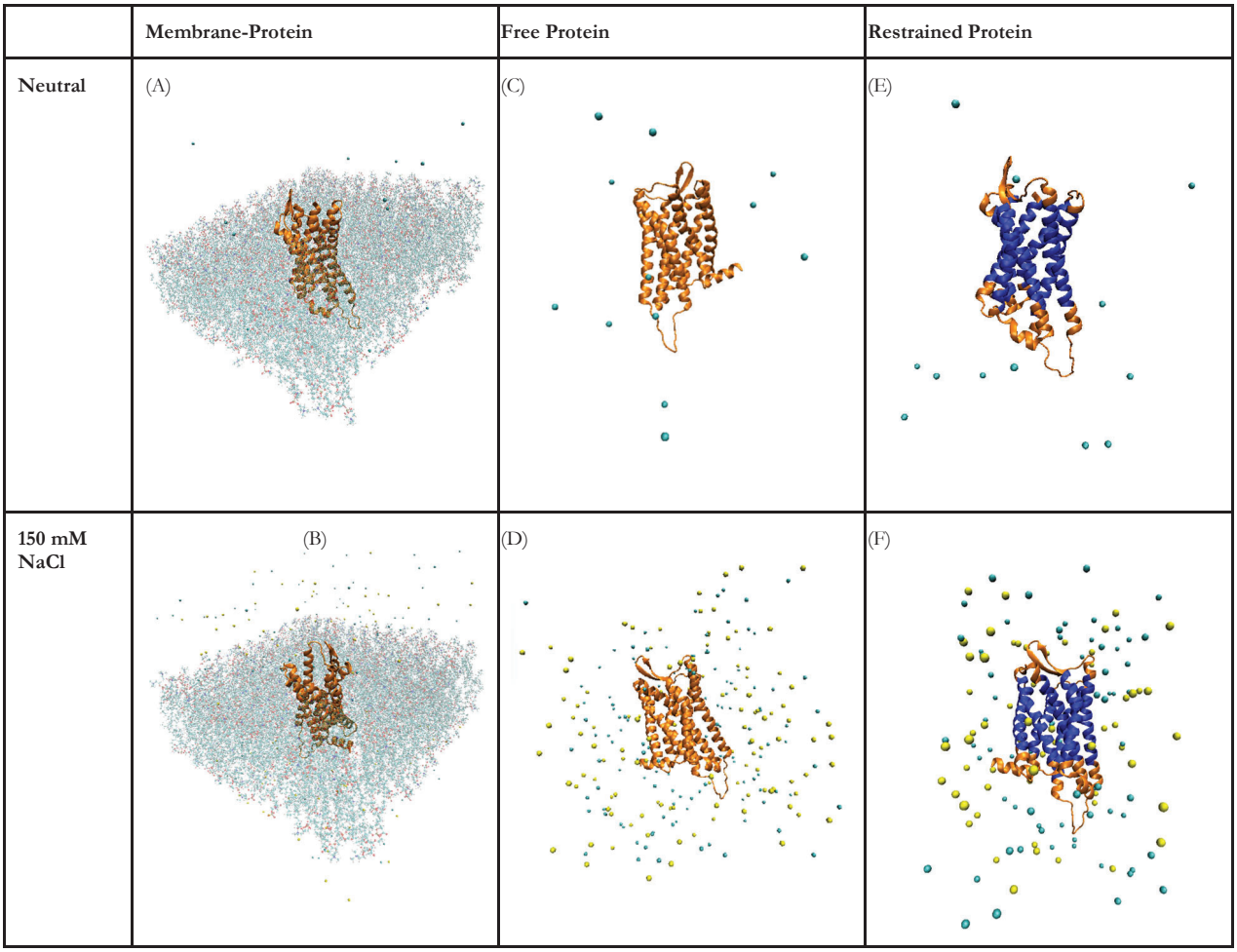

Figure 2. Summary of simulation setups. Although explicitly modeled, water molecules are not shown for clarity. Sodium ions are shown as yellow beads and chlorine ions are shown as blue beads (A) MOR (orange) is simulated in an explicit lipid bilayer with 22.5 Å of water on the top and bottom of the membrane. 13 chlorine ions are added to neutralize the system. (B) MOR (orange) is simulated in an explicit lipid bilayer with 22.5 Å of water on the top and bottom of the membrane and 150 mM sodium chloride. (C) The free MOR is simulated in a 111 Å^3 water box neutralized with 13 chlorine ions. (D) The free MOR is simulated in a 111 Å^3 water box with 150 mM sodium chloride. (E) MOR is simulated within an orthorhombic box with a 16 Å water buffer and transmembrane residues (blue) restrained. 13 chlorine ions are added to neutralize the system. (F) MOR is simulated within an orthorhombic box with a 16Å water buffer and 150 mM sodium chloride. Transmembrane residues (blue) are restrained.

Each of the three systems were solvated in water with 13 chlorine counterions to neutralize the system and in a 150 mM NaCl solution. Systems containing 13 chlorine counterions and no NaCl will be referred to as "neutral pH" and systems with 13 chlorine counterions and 150 mM NaCl will be referred to as "150 mM NaCl". In all the systems solvated with NaCl, the allosteric sodium ion was manually moved to its binding site at the midpoint of D114 and S154. The box dimensions for each simulation are summarized in **Table 1**.

Atomistic molecular dynamics simulations were performed using the NAMD 3.0 alpha software package.[30] The CHARMM36m

force field[31] was used to model the protein and the CHARMM C36 lipid force field[32] was used to model the membrane. Throughout all of the simulations, the SETTLE algorithm[33] was used to constrain bonds that include a hydrogen atom and a 2 fs time step was employed. In all simulations, a switching distance of 10 Å and cutoff of 12 Å was used for all nonbonded interactions. Long-range electrostatics beyond the nonbonded cutoff of 12 Å were calculated using the particle mesh Ewald (PME) summation. All simulations were performed at 303.15 K. Each simulation was performed using one NVIDIA A100 Tensor Core GPU on Hipergator 3.0.

	Membrane-Protein	**Free Protein**	**Restrained Protein**
Box Dimensions	120 Å×120 Å×125 Å	111 Å×111 Å×111 Å	81 Å×73 Å×111 Å

Table 1. Box dimensions for each system setup.

The membrane-protein systems were minimized for 10,000 steps using the conjugate gradient algorithm with harmonic and dihedral restraints on the protein and lipid and a planar restraint on the membrane. The system was gradually heated from 0 to 303.15 K in an NVT (constant number of atoms, volume, and temperature) ensemble with harmonic restraints on protein and lipids. Minimization was followed by six steps of equilibration with NPAT (constant number of atoms, pressure, lipid bilayer area, and temperature) dynamics. During equilibration, harmonic restraints were applied to the ions and protein backbone and planar restraints were used to prevent water from entering the membrane and to hold the lipid head groups in the plane of the Z-axis. Restraint force constants used during minimization and equilibration are summarized in **Table 2**. Production simulations were performed in a NPAT ensemble with pressure only changing in the Z direction using the Langevin thermostat with a $1ps^{-1}$ collision frequency and Nosé-Hoover Langevin barostat with a timestep of 2 fs.

Step	**Ensemble**	**Time (ps)**	**Backbone Heavy Atoms Restraint***	**Sidechain Heavy Atoms Restraint***	**Lipid Position Restraint***	**Lipid Dihedral Restraint***
Minimization	NVT	20	10	5.0	5	500
1	NPT	250	10	5.0	5	500
2	NPAT	250	5.0	2.5	5	200
3	NPAT	500	2.5	1.25	2	100
4	NPAT	500	1.0	0.5	1	100
5	NPAT	500	0.5	0.25	0.2	50
6	NPAT	500	0.1	0.05	0	0

Table 2. Summary of minimization and equilibration setup for the membrane-protein system. *All units for restraint constants are in kcal/mol/Å^2

The free protein systems were minimized for 10,000 steps using the conjugate gradient algorithm with a 20 kcal/mol/Å^2 harmonic force restraining the protein backbone and the system was heated from 0 K to 303.15 K in an NVT ensemble. This was followed by four stages of equilibration, each lasting 25,000 steps, with the harmonic restraint constant being gradually decreased from 20 kcal/mol/Å^2 to 10 kcal/mol/Å^2 to 5 kcal/mol/Å^2 to 2.5 kcal/mol/Å^2 in an NPT (constant number of atoms, pressure, and temperature) ensemble with a 2 fs time step. The production data was generated using an NPT ensemble at 303.15 K and 1 atm using the Langevin thermostat with a 1 ps^{-1} collision frequency and Nosé-Hoover Langevin barostat with a 2 fs time step and coordinates and system properties output every 10 ps.

The restrained protein simulations were minimized and heated using the same methods as the free protein systems. This was followed by four stages of equilibration, each lasting 25,000 steps with the protein restraint being gradually decreased from 20 kcal/mol/Å^2 to the desired restraint in an NPT ensemble with a 2 fs time step. The production simulations were performed with a harmonic restraining force applied to all atoms in transmembrane residues of MOR from the protein with PDB ID: 4DKL.[34] The harmonic restraining forces reduce mobility by adding an extra energetic penalty defined by **Equation 1**.

$$U(x) = k(x - x_{ref})^2 \qquad \textbf{Equation 1.}$$

Where x is the position of an atom at a given time, x_{ref} is the position of that atom at the first frame of minimization and k is the force constant. As mentioned above, the force constants used in this study were 20 kcal/mol/Å^2, 5 kcal/mol/Å^2, 1 kcal/mol/Å^2, 0.01 kcal/mol/Å^2 and 0.001 kcal/mol/Å^2, and were applied during production simulation to all atoms in the transmembrane region of MOR. Other than the restraints, production data was generated using the same methods as the free protein systems.

For all systems, results were generated from simulations of 1000 ns with the first 200 ns being considered as equilibration and not included in calculations of average values. System properties were output every 50000 steps. The root mean square deviation (RMSD) and root mean squared fluctuation (RMSF) were calculated using cpptraj.[35] In this study, the RMSD is a measure of the difference between the protein coordinates at a reference state, and the protein coordinates at a given timestep. The RMSD is calculated by

$$RMSD = \sqrt{\sum_{i=0}^{N} \frac{m_i(X_i - Y_i)^2}{M}} \qquad \textbf{Equation 2.}$$

Where m_i is the mass of a given atom, X_i is the position of a given atom, Y_i is the reference position of a given atom and M is the total mass of the system. In this work, RMSDs are calculated for the backbone atoms (nitrogen, carbon, and alpha carbon) and the first frame after minimization and heating is used as the reference structure.

The RMSF is the time average of the RMSD and is calculated for each individual residue. The RMSF for an atom X_i is calculated by

$$RMSF = \sqrt{\langle (X_i - \langle X_i \rangle)^2 \rangle} \qquad \textbf{Equation 3.}$$

Where X_i is the coordinates of as particle and $\langle X_i \rangle$ is the average position of that particle. In this work RMSF is calculated for backbone atoms using the first frame after minimization and heating as the reference structure.

Additionally, the distributions of the χ_1 and χ_2 angles of N332 were calculated using cpptraj.[35] The χ_1 angle is the torsional angle including the nitrogen, α-carbon, β-carbon, and γ-carbon of N332 and the χ_2 angle is the torsional angle involving the α-carbon, β-carbon, and γ-carbon, and δ-oxygen of N332. The confirmation of these torsional angles has been shown to be related to the downstream signaling of the receptor.[13]

All error values are reported as a 95% confidence interval which is calculated as $\pm$ 1.96σ, where σ is the standard deviation.

RESULTS AND DISCUSSION

The RMSD of the systems studied in this work are shown in **Figure 3**. To note, the RMSD of the free MOR system (**Figure 3**, panel B) is higher than the RMSD of MOR in its explicitly modeled lipid bilayer (**Figure 3**, panel A). The average RMSD of the free protein is 3.9 ± 0.5 Å and 3.4 ± 0.6 Å for the neutral system and system with 150 mM NaCl respectively, compared to the membrane-protein system which has an average RMSD of 3.1 ± 0.6 Å and 3.2 ± 0.3 Å for the neutral system and system with 150 mM NaCl respectively (**Table 3**). Thus, as expected, the protein moves more freely in the absence of the lipid bilayer. This is because the amino acids in the transmembrane regions of the lipid-free MOR are not structurally stabilized by the viscous lipid bilayer, allowing more freedom of motion. However, adding restraints to the transmembrane region lowers the overall RMSD (**Figure 3**, panel C) for all of the restraint force constants tested. The RMSD of the protein with the 0.001 kcal/mol/Å^2 restraint force constant is closest to the RMSD of the protein with its explicitly modeled lipid bilayer (**Table 3**). Systems with higher restraint force constants (0.01–20 kcal/mol/Å^2) all have lower average RMSD values than the membrane-protein system. Additionally, the RMSD of systems simulated with 150 mM of NaCl tend to have a lower RMSD than systems in neutral conditions without the allosteric sodium ion; this is in agreement with previous studies that show that the allosteric sodium ion stabilizes MOR into its inactive state.[11, 12]

System	RMSD of System with Neutral pH (Å)	RMSD of System with 150 mM NaCl (Å)
Free Protein	3.9 ± 0.5	3.4 ± 0.6
Membrane-Protein	3.1 ± 0.6	3.2 ± 0.3
MOR with Restraints on Transmembrane Atoms		
20 kcal/mol/Å²	1.9 ± 0.5	2.2 ± 0.4
5 kcal/mol/Å²	2.3 ± 0.6	2.1 ± 0.5
1 kcal/mol/Å²	2.3 ± 0.6	2.2 ± 0.5
0.01 kcal/mol/Å²	2.4 ± 0.6	2.9 ± 1.0
0.001 kcal/mol/Å²	3.1 ± 0.5	3.0 ± 0.4

Table 3. Summary of average RMSDs for each system. The average RMSD is calculated from the last 800 ns of simulation and error is reported as the 95% confidence interval.

To better understand how the dynamic properties of MOR differ in the three models, the RMSD was calculated only for the transmembrane residues, *i.e.*, residues 67 to 91, 105 to 129, 141 to 163, 184 to 205, 229 to 253, 278 to 304, and 313 to 336 and represented in **Figure 4** and **Table 4**. This shows that the RMSD of the transmembrane residues of the free MOR are 1–1.3 Å higher than in MOR in an explicitly modeled lipid bilayer. The average transmembrane RMSDs in the free protein system are 3.2 ± 0.4 Å and 2.3 ± 0.6 Å for the neutral system and the system with 150 mM NaCl respectively, compared to 1.9 ± 0.3 Å and 1.3 ± 0.2 Å in the system with the explicitly modeled lipid bilayer (**Table 4**).

Addition of restraints successfully lowers the RMSD of the transmembrane residues as shown in **Figure 4**, panel C. However, the systems with 1 kcal/mol/Å², 5 kcal/mol/Å², and 20 kcal/mol/Å² restraint constants have drastically lower RMSDs in the transmembrane region (**Table 4**) and do not accurately model the dynamics of MOR in an explicitly modeled lipid bilayer. The protein with the 0.01 kcal/mol/Å² restraint constant is also notably lower than that of MOR in its explicitly modeled lipid bilayer. However, the protein with the 0.001 kcal/mol/Å² restraint constant has a transmembrane RMSD that differs only by 0.3 Å from the membrane-protein system for both the neutral system and the system with 150 mM NaCl. Throughout the simulations, the transmembrane RMSD of the systems with the allosteric sodium ion tend to be lower due to its stabilizing effect on the inactive MOR.[11, 12]

System	RMSD of Transmembrane Atoms of System with Neutral pH (Å)	RMSD of Transmembrane Atoms of System with 150 mM NaCl (Å)
Free Protein	3.2 ± 0.4	2.3 ± 0.6
Membrane-Protein	1.9 ± 0.3	1.3 ± 0.2
MOR with Restraints on Transmembrane Atoms		
20 kcal/mol/Å²	0.12 ± 0.01	0.13 ± 0.01
5 kcal/mol/Å²	0.27 ± 0.02	0.18 ± 0.02
1 kcal/mol/Å²	0.27 ± 0.02	0.28 ± 0.02
0.01 kcal/mol/Å²	0.92 ± 0.11	0.87 ± 0.15
0.001 kcal/mol/Å²	1.6 ± 0.3	1.6 ± 0.3

Table 4. Summary of average RMSDs of transmembrane residues for each system. The average RMSD is calculated from the last 800ns of simulation and error is reported as the 95% confidence interval.

The RMSF of each system is analyzed to showcase the impact of each system setup in different regions of the protein and shown in **Figure 5**. Across all residues, the free MOR tends to have a higher RMSF than the membrane-protein system.

Of the systems with transmembrane restraints, the system with the 0.001 kcal/mol/Å² restraint force constant has an RMSF that most closely models the membrane-protein system in the transmembrane region. However, the protein with the 0.001 kcal/mol/Å² restraint force constant tends to have a higher RMSF in the intra and extracellular regions than the membrane protein system. Particularly, the RMSF of residues 254-277, which are highlighted in purple on **Figure 6**, and residues 305-312, which are highlighted in green on **Figure 6**, are higher in the restrained protein system than the membrane-protein system. It is possible that the higher RMSF in the system with the 0.001 kcal/mol/Å² restraint force constant could be due to differences caused by the lack of an explicitly modeled lipid bilayer. However, both of these regions are mostly in a random coil structure and therefore more flexible than other regions of the protein, providing a possible explanation for greater differences between simulations.

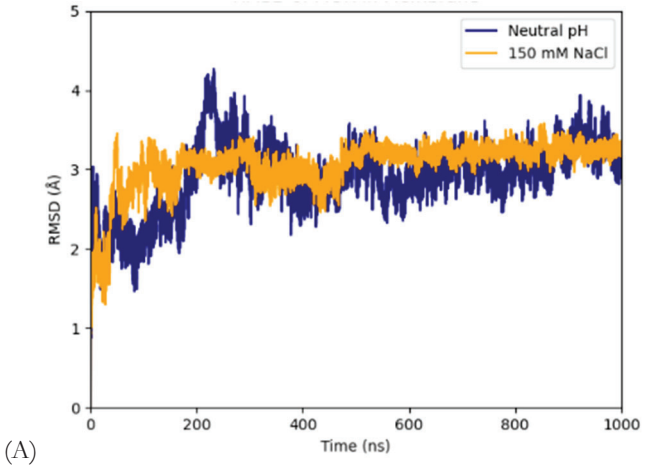

(A)

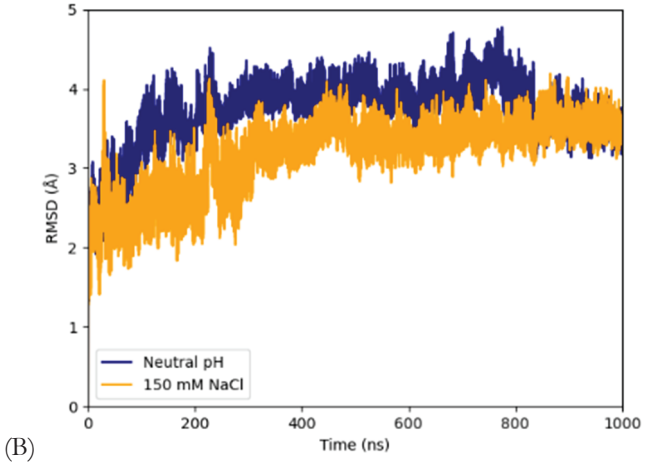

(B)

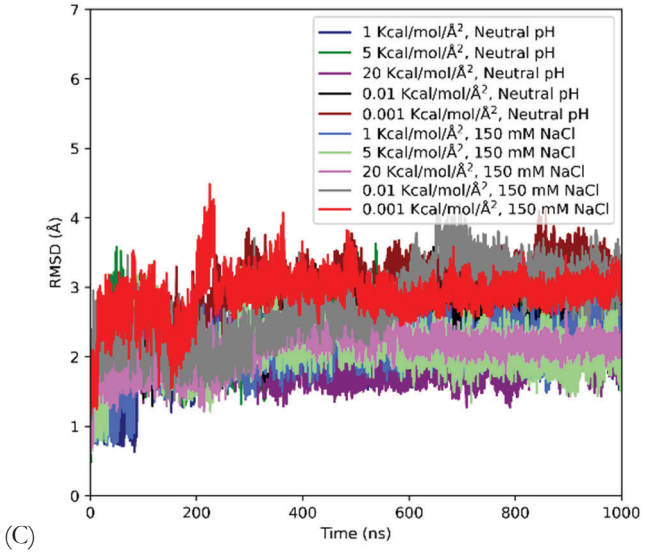

(C)

Figure 3. (A) The RMSD of MOR in an explicitly modeled lipid bilayer (B) The RMSD of the free MOR (C) The RMSD of MOR with restraints

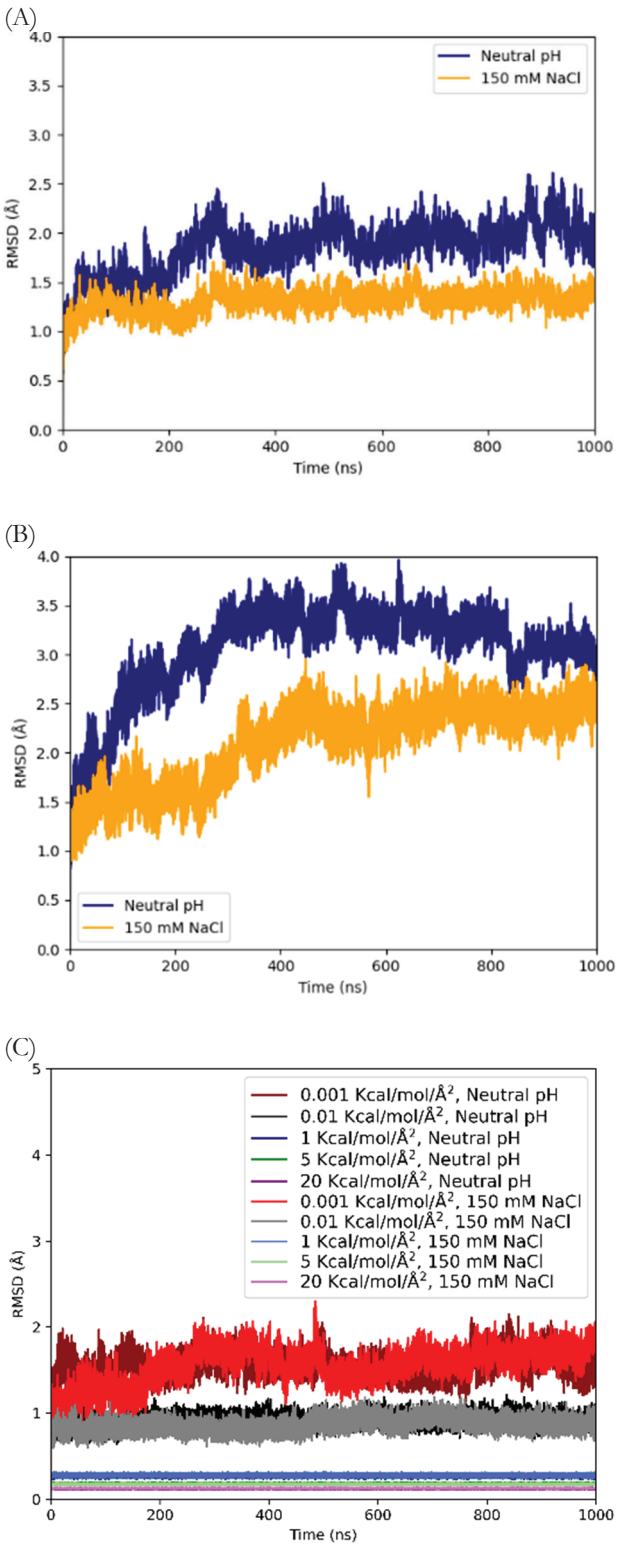

Figure 4. (A) The RMSD of transmembrane residues of the membrane-protein system (B) The RMSD of transmembrane residues of the free MOR (C) The RMSD of transmembrane residues of MOR with restraints.

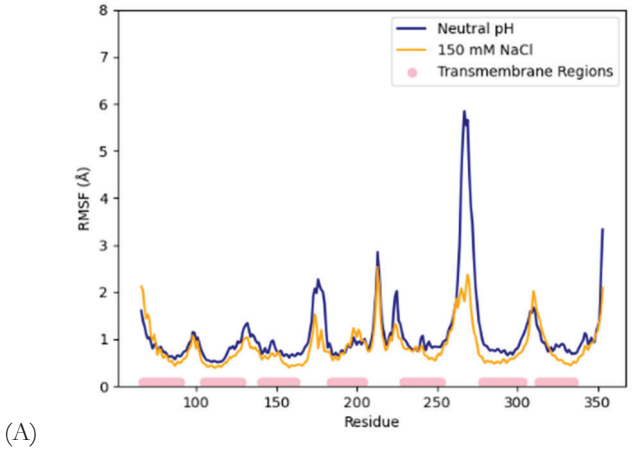

(A)

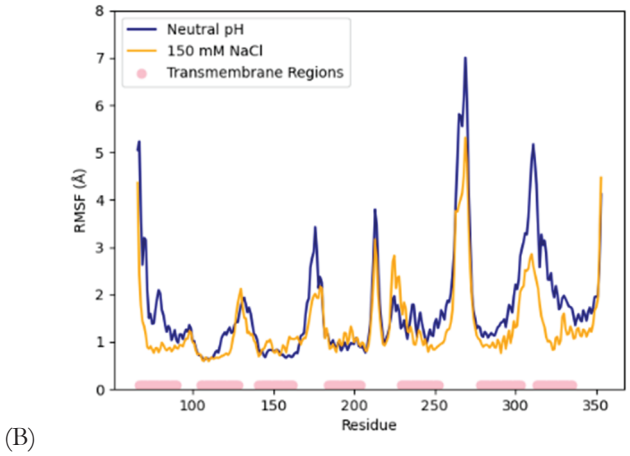

(B)

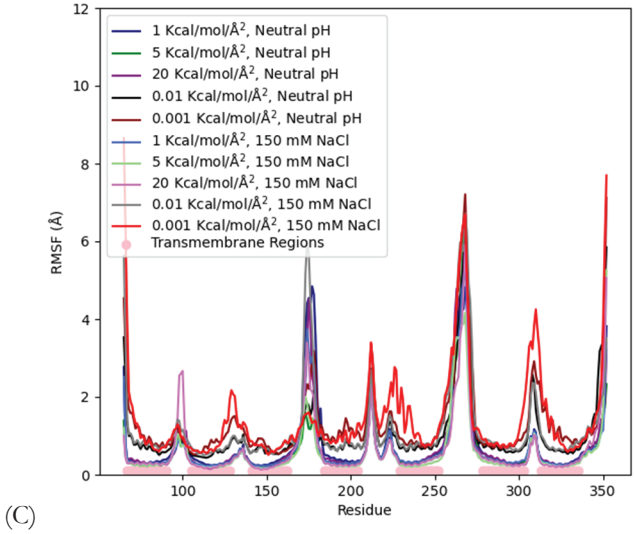

(C)

Figure 5. All RMSFs are calculated from the last 800 ns of simulation data. The transmembrane residues are highlighted in pink. (A)The RMSF of MOR in the membrane-protein system (B) The RMSF of the free MOR (C) The RMSF of the restrained MOR

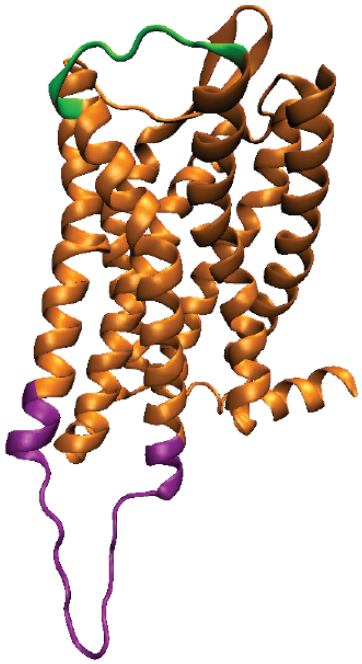

Figure 6. MOR with regions of interest highlighted. Residues 254-277 are highlighted in purple and residues 305-312 are highlighted in green.

The impact of each method of modeling the lipid bilayer on the NPxxY motif was analyzed by calculating distributions of side-chain dihedral angles χ_1 and χ_2 of N332, shown in **Figure 7**. The conformation of the side-chain dihedral angles of N332 have been shown to be related with the downstream signaling of the receptor.[13]

In the system simulated with an explicitly modeled lipid bilayer, the χ_1 dihedral distribution has peaks near -75 and -180 degrees in the neutral system, and a peak at -75 in the system with 150 mM NaCl. In both the free MOR system and system with restraints on the transmembrane residues a peak at -80 degrees is observed in both the neutral system and the system with 150 mM NaCl. In the neutral free MOR system and neutral system with a 0.001kcal/mol/Å^2 restraint force constant, a peak is noticeable at -180 degrees, but the peak is smaller than the one observed in the system with the explicitly modeled lipid bilayer.

The χ_2 dihedral distribution of the system simulated with the explicitly modeled lipid bilayer has peaks of -20, and -115 degrees for the neutral system and a peak at -20 degrees for the system with 150 mM NaCl. Both the free MOR system and system with restraints on the transmembrane residues have peaks at -20 degrees for both the neutral and systems with -150 mM NaCl. A small peak at -115 degrees is observed in both the neutral free MOR system and the neutral system with a 0.001kcal/mol/Å^2 restraint force constant.

Ultimately, the systems with a 0.001kcal/mol/Å^2 restraint force constant on the transmembrane residues are able to capture the peaks in the distribution of the χ_1 and χ_2 torsion angles of N332. Because the χ_1 and χ_2 torsion angles of N332 are associated with the downstream signaling of MOR, this analysis should be used in future simulations containing the receptor a ligand bound state to validate the system with transmembrane restraints' ability to capture differences associated with downstream signaling.[13]

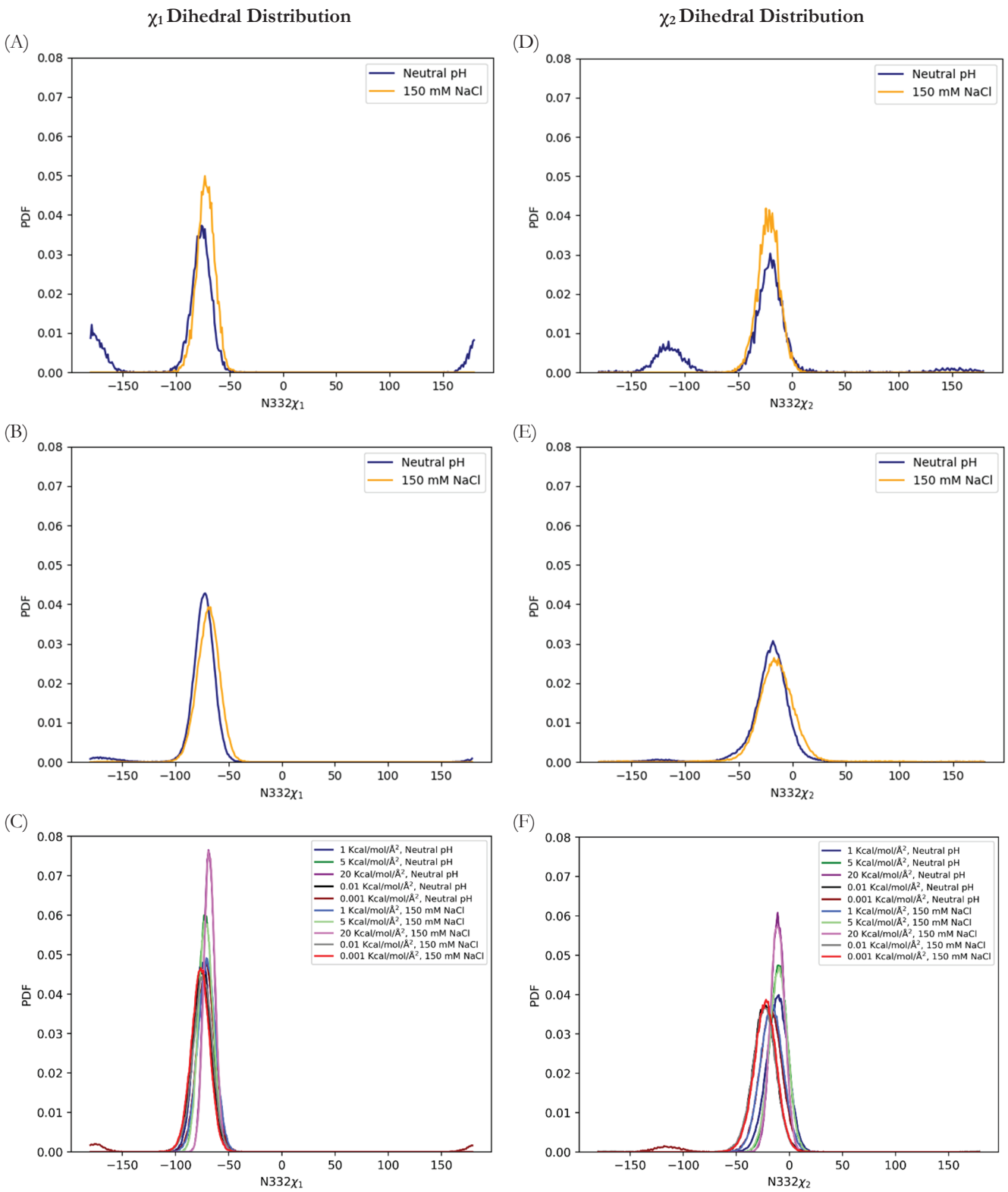

Figure 7. Dihedral distributions of the χ_1 (A-C) and χ_2 (D-F) angle of N332 are calculated from the last 800 ns of simulation data. (A) The dihedral distributions of the χ_1 angle of N332 of MOR in the membrane-protein system (B) The dihedral distributions of the χ_1 angle of N332 of the free MOR (C) The dihedral distributions of the χ_1 angle of N332 of the restrained MOR (D) The dihedral distributions of the χ_2 angle of N332 of MOR in the membrane-protein system (E) The dihedral distributions of the χ_2 angle of N332 of the free MOR (F) The dihedral distributions of the χ_2 angle of N332 of the restrained MOR

The values reported in this work for RMSD and transmembrane RMSD agree with values reported in literature. Ricarte *et al.* reports a total RMSD for MOR bound to morphine of 2.9-3.2 Å based on three simulations of 2-3 μs.[36] This coincides with the values reported in this work of 3.1-3.2 Å for the membrane-protein system and 3.0-3.1 Å for the system with 0.001 kcal/mol/Å^2 restraint constant. Cong *et al.* reports a transmembrane RMSD of 1.7, 1.3 and 1.2 Å for MOR bound to morphine, hydromorphone and β-funaltrexamine respectively[37], which agrees with the transmembrane RMSDs of 1.3-1.9 Å for the membrane-protein system and 1.6 Å for the system with 0.001 kcal/mol/Å^2 restraint force constant. One difference between the simulations in this work and the literature values summarized here is the presence of morphine bound to MOR. However, other simulations show that morphine does not have a dramatic impact on the RMSD of MOR.[38] Another difference between the results summarized here is that MOR was simulated in a membrane of 100% POPC whereas in this work MOR was simulated in a membrane of 90% POPC and 10% cholesterol. Short 200 ns simulations were performed using the same simulation setup outlined in this paper but with a membrane of 100% POPC to evaluate the role of bilayer composition on receptor dynamics. These simulations showed that the POPC membrane did not cause a dramatic difference in RMSD within the timescale, suggesting that the restrained-protein model may be appropriate to model bilayers with a range of POPC/cholesterol ratios (Supplemental Information, **Figure S1**).

Despite accurately modeling overall structural properties of MOR in its explicitly modeled lipid bilayer, there are some limitations to the restrained protein model. It has been shown that cholesterol can bind to residues on TM6 and TM7 of MOR affecting the likelihood of β-arrestin recruitment.[39] Without explicitly modeling the lipid bilayer, the impact of cholesterol binding cannot be modeled using the system proposed in this study. Additionally, experimental work has shown that different ligands bound to MOR can affect the protein's mobility perpendicular to the lipid bilayer.[40] Because the residues with restraints applied remain constant throughout the simulation, this is a feature of MOR-ligand interactions that could not be studied using the restrained protein model.

Since the restrained protein system with a 0.001 kcal/mol/Å^2 restraint force constant accurately models the dynamic properties of MOR in its explicitly modeled lipid bilayer, it is important to assess the relative computational efficiency of these systems. The restrained protein system is able to generate 49% faster than the system with the explicitly modeled lipid bilayer (**Figure 8**). The restrained protein system has the fewest number of atoms because it does not contain an explicitly modeled lipid bilayer, and the smaller size of the system contributes to increased simulation speed. This shows that using a backbone restraint on transmembrane residues can speed up data generation and increase the length of simulations of MOR.

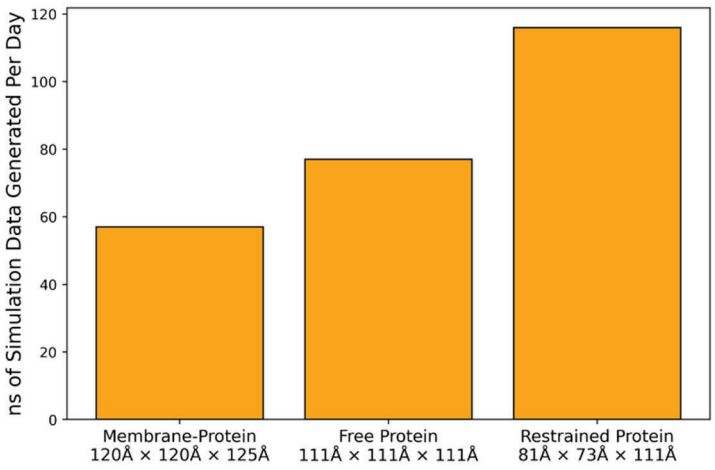

Figure 8. Nanoseconds of simulation data generated per day for each system.

CONCLUSIONS

This work shows that the free MOR in water has a higher RMSD than MOR in its explicitly modeled lipid bilayer, particularly in the transmembrane regions. Comparisons between MOR in its explicitly modeled lipid bilayer and MOR with varying restraints applied to its transmembrane residues show that using a restraint force constant of 0.001 kcal/mol/Å^2 on the transmembrane residues of MOR can model the overall dynamic properties of the membrane-protein system. The average RMSD values of MOR in its explicitly modeled lipid bilayer are reproduced within 95% confidence intervals by the corresponding systems simulated with a restraint force constant of 0.001 kcal/mol/Å^2 on the transmembrane residues.

The RMSF does differ between the restraint model and the membrane-protein model in the intra and extracellular regions, particularly residues 254-277 and residues 305-312, which is likely due to the highly flexible nature of this region. Additionally, analysis of the distribution of the χ_1 and χ_2 angles of N332 showed that simulations of the MOR with a 0.001kcal/mol/Å^2 restraint force constant on the transmembrane residues are able to capture the distributions seen in the system with an explicitly modeled lipid bilayer. Importantly, while using the restrained model data is generated twice as quickly as the explicit membrane model. With further validation of simulations using membranes on the transmembrane residues to simulate MOR bound to ligands, this method may be an effective approach to model overall structural properties of MOR, allowing for a faster screening of new opioid drug molecules.

In order to explore the applications of the restrained protein model in studies involving new opioid molecules and to assess its ability to model drug-induced protein dynamics, an opioid agonist such as morphine can be docked to the crystal structure of MOR using e.g., AutoDock Vina[41, 42] to create a starting structure that approximates the ligand's binding pose. The 3-dimensional structures of drug molecules can be taken from the Zinc Database. Parameters should be developed for the drug molecules using software such as the ParamChem[43, 44] tool for CGENFF 2.5.[45] The accuracy of the parameters for the drug molecules should also be assessed based on a comparison of the computational binding free energy with experimental data. If necessary, parameters can be further optimized using the ForceField Toolkit in VMD.[46, 47] Once the parameters have been validated, they can then be used to perform molecular dynamics simulations of at least 500 ns of the drug-receptor complex both in an explicitly modeled lipid bilayer and with a restraint force constant of 0.001 kcal/mol/Å^2 applied to the transmembrane residues. The results of the membrane-protein simulation and the restrained protein simulation should be compared to assess if the restrained model is able to represent protein dynamics associated with ligand binding.

ACKNOWLEDGEMENTS

Part of this research was financially supported by the University Scholars Program awarded to Allison Barkdull. Additionally, the authors thank the University of Florida Department of Chemistry and The J. Crayton Pruitt Family Department of Biomedical Engineering. Computational resources utilized were managed by the University of Florida (HiPerGator 3.0).

REFERENCES

1. CDC Injury Center, U.S. Opioid Dispensing Rate Maps | Drug Overdose | *https://www.cdc.gov/drugoverdose/rxrate-maps/index.html* (Accessed April 2022)

2. Minami, M. and Satoh, M. (1995) Molecular Biology of the Opioid Receptors: Structures, Functions and Distributions, *Neurosci. Res.* 23 (2), 121–145. *https://doi.org/10.1016/0168-0102(95)00933-k*

3. Ciccarone, D. (2021) The Rise of Illicit Fentanyls, Stimulants and the Fourth Wave of the Opioid Overdose Crisis, *Curr. Opin. Psychiatry.* 34 (4), 344–350. *https://doi.org/10.1097/yco.0000000000000717*

4. Matthes, H. W. D., Maldonado, R., Simonin, F., Valverde, O., Slowe, S., Kitchen, I., Befort, K., Dierich, A., Le Meur, M., Dollé, P., Tzavara, E., Hanoune, J., Roques, B. P., and Kieffer, B. L. (1996) Loss of Morphine-Induced Analgesia, Reward Effect and Withdrawal Symptoms in Mice Lacking the μ-Opioid-Receptor Gene, *Nature* 383 (6603), 819–823. *https://doi.org/10.1038/383819a0*

5. Minami, M., and Satoh, M. (1995) Molecular Biology of the Opioid Receptors: Structures, Functions and Distributions, *Neurosci. Res. 23* (2), 121–145. *https://doi.org/10.1016/0168-0102(95)00933-k*

6. Weis, W. I., and Kobilka, B. K. (2008) Structural Insights into G-Protein-Coupled Receptor Activation, *Curr. Opin. Struct. Biol.* 18 (6), 734–740. *https://doi.org/10.1016/j.sbi.2008.09.010*

7. Raehal, K. M., Schmid, C. L., Groer, C. E., and Bohn, L. M. (2011) Functional Selectivity at the μ-Opioid Receptor: Implications for Understanding Opioid Analgesia and Tolerance, *Pharmacol. Rev.* 63 (4), 1001–1019. *https://doi.org/10.1124/pr.111.004598*

8. Raffa, R. B., Martinez, R. P., and Connelly. (1994) C. D. G-Protein Antisense Oligodeoxyribonucleotides and μ-Opioid Supraspinal Antinociception, *Eur. J. Pharmacol.* 258(1-2), R5–R7. *https://doi.org/10.1016/0014-2999(94)90073-6*

9. Jordan, B., and Devi, L. A. (1998) Molecular Mechanisms of Opioid Receptor Signal Transduction. *Br. J. Anaesth.* 81 (1), 12–19. *https://doi.org/10.1093/bja/81.1.12*

10. Fenalti, G., Giguere, P. M., Katritch, V., Huang, X.-P., Thompson, A. A., Cherezov, V., Roth, B. L., and Stevens, R. C. (2014) Molecular Control of δ-Opioid Receptor Signalling, *Nature* 506 (7487), 191–196. *https://doi.org/10.1038/nature12944*

11. Katritch, V., Fenalti, G., Abola, E. E., Roth, B. L., Cherezov, V., and Stevens, R. C. (2014) Allosteric Sodium in Class a GPCR Signaling, *Trends Biochem. Sci.* 39 (5), 233–244. *https://doi.org/10.1016/j.tibs.2014.03.002*

12. Selley, D. E., Cao, C.-C., Liu, Q., and Childers, S. R. (2000) Effects of Sodium on Agonist Efficacy for G-Protein Activation in μ-Opioid Receptor-Transfected CHO Cells and Rat Thalamus. *Br. J. Pharmacol.* 130 (5), 987–996. *https://doi.org/10.1038/sj.bjp.0703382*

13. Marmolejo-Valencia, A. F., Madariaga-Mazón, A., and Martinez-Mayorga, K. (2021) Bias-Inducing Allosteric Binding Site in Mu-Opioid Receptor Signaling, *SN Appl. Sci.* 3 (5). https://doi.org/10.1007/s42452-021-04505-8.

14. Marmolejo-Valencia, A. F., and Martínez-Mayorga, K. (2017) Allosteric Modulation Model of the Mu Opioid Receptor by Herkinorin, a Potent Not Alkaloidal Agonist, *J. Comput. Aided Mol. Des.* 31 (5), 467–482. *https://doi.org/10.1007/s10822-017-0016-7*

15. Huang, W., Manglik, A., Venkatakrishnan, A. J., Laeremans, T., Feinberg, E. N., Sanborn, A. L., Kato, H. E., Livingston, K. E., Thorsen, T. S., Kling, R. C., Granier, S., Gmeiner, P., Husbands, S. M., Traynor, J. R., Weis, W. I., Steyaert, J., Dror, R. O., and Kobilka, B. K. (2015) Structural Insights into μ-Opioid Receptor Activation, *Nature* 524 (7565), 315–321. *https://doi.org/10.1038/nature14886*

16. Manglik, A., Kruse, A. C., Kobilka, T. S., Thian, F. S., Mathiesen, J. M., Sunahara, R. K., Pardo, L., Weis, W. I., Kobilka, B. K., and Granier, S. (2012) Crystal Structure of the μ-Opioid Receptor Bound to a Morphinan Antagonist, *Nature* 485 (7398), 321–326. *https://doi.org/10.1038/nature10954*

17. Shang, Y., LeRouzic, V., Schneider, S., Bisignano, P., Pasternak, G. W., and Filizola, M. (2014) Mechanistic Insights into the Allosteric Modulation of Opioid Receptors by Sodium Ions, *Biochemistry* 53 (31), 5140–5149. *https://doi.org/10.1021/bi5006915*

18. Hernández-Alvarado, R. B., Madariaga-Mazón, A., Cosme-Vela, F., Marmolejo-Valencia, A. F., Nefzi, A., and Martinez-Mayorga, K. (2021) Encoding Mu-Opioid Receptor Biased Agonism with Interaction Fingerprints, *J. Comput. Aided Mol. Des.* 35 (11), 1081–1093. *https://doi.org/10.1007/s10822-021-00422-5*

20. Shen, R., Han, W., Fiorin, G., Islam, S. M., Schulten, K., & Roux, B. (2015). Structural Refinement of Proteins by Restrained Molecular Dynamics Simulations with Non-interacting Molecular Fragments. *PLOS Comput. Biol. 11*(10), e1004368. https://doi.org/10.1371/journal.pcbi.1004368

21. Sansom, M. S. P., Sankararamakrishnan, R., and Kerr, I. D. (1995). Modelling membrane proteins using structural restraints. *Nature Structural Biology*, *2*(8), 624–631. https://doi.org/10.1038/nsb0895-624

21. Niesen, M. J. M., Bhattacharya, S., and Vaidehi, N. (2011) The Role of Conformational Ensembles in Ligand Recognition in G-Protein Coupled Receptors, *J. Am. Chem. Soc.*133 (33), 13197–13204. *https://doi.org/10.1021/ja205313h*

22. Manglik, A., Kruse, A. C., Kobilka, T. S., Thian, F. S., Mathiesen, J. M., Sunahara, R. K., Pardo, L., Weis, W. I., Kobilka, B. K., and Granier, S. (2012) Crystal Structure of the Mu-Opioid Receptor Bound to a Morphinan Antagonist. *https://doi.org/10.2210/pdb4dkl/pdb*

23. Huang, W. J., Manglik, A., Venkatakrishnan, A. J., Laeremans, T., Feinberg, E. N., Sanborn, A. L., Kato, H. E., Livingston, K. E., Thorsen, T. S., Kling, R., Granier, S., Gmeiner, P., Husbands, S. M., Traynor, J. R., Weis, W. I., Steyaert, J., Dror, R. O., and Kobilka, B. K. (2015) Crystal Structure of Active Mu-Opioid Receptor Bound to the Agonist BU72. *https://doi.org/10.2210/pdb5c1m/pdb*

24. Kaufman, Daniel L., et al. (1995) Characterization of the Murine μ Opioid Receptor Gene, *Journal of Biological Chemistry.* 270 (26), 15877–15883. https://doi.org/10.1074/jbc.270.26.15877.

25. Mestek, A, et al. (1995) The Human Mu Opioid Receptor: Modulation of Functional Desensitization by Calcium/Calmodulin-Dependent Protein Kinase and Protein Kinase C, *The Journal of Neuroscience.* 15 (3), 2396–2406. https://doi.org/10.1523/jneurosci.15-03-02396.1995.

26. Needleman, Saul B., and Christian D. Wunsch. (1970) A General Method Applicable to the Search for Similarities in the Amino Acid Sequence of Two Proteins, *Journal of Molecular Biology.* 48 (3), 443–453. https://doi.org/10.1016/0022-2836(70)90057-4.

27. Lee, J., Patel, D. S., Ståhle, J., Park, S.-J., Kern, N. R., Kim, S., Lee, J., Cheng, X., Valvano, M. A., Holst, O., Knirel, Y. A., Qi, Y., Jo, S., Klauda, J. B., Widmalm, G., and Im, W. (2018) CHARMM-GUI Membrane Builderfor Complex Biological Membrane Simulations with Glycolipids and Lipoglycans, *J. Chem. Theory Comput.* 15 (1), 775–786. *https://doi.org/10.1021/acs.jctc.8b01066*

28. Jorgensen, W. L., Chandrasekhar, J., Madura, J. D., Impey, R. W., and Klein, M. L. (1983) Comparison of Simple Potential Functions for Simulating Liquid Water, *J. Chem. Phys.* 79 (2), 926–935. https://doi.org/10.1063/1.445869

29. Jorgensen, W. L., Chandrasekhar, J., Madura, J. D., Impey, R. W., and Klein, M. L. (1983) Comparison of Simple Potential Functions for Simulating Liquid Water, *J. Chem. Phys.* 79 (2), 926–935. https://doi.org/10.1063/1.445869

30. Phillips, J. C., Braun, R., Wang, W., Gumbart, J., Tajkhorshid, E., Villa, E., Chipot, C., Skeel, R. D., Kalé, L., and Schulten, K. (2005) Scalable Molecular Dynamics with NAMD, *J. Comput. Chem.* 26 (16), 1781–1802. *https://doi.org/10.1002/jcc.20289*

31. Huang, J., Rauscher, S., Nawrocki, G., Ran, T., Feig, M., de Groot, B. L., Grubmüller, H., and MacKerell, A. D. (2016) CHARMM36m: An Improved Force Field for Folded and Intrinsically Disordered Proteins, *Nat. Methods* 14 (1), 71–73. *https://doi.org/10.1038/nmeth.4067*

32. Klauda, J. B., Venable, R. M., Freites, J. A., O'Connor, J. W., Tobias, D. J., Mondragon-Ramirez, C., Vorobyov, I., MacKerell, A. D., and Pastor, R. W. (2010) Update of the CHARMM All-Atom Additive Force Field for Lipids: Validation on Six Lipid Types, *J. Phys. Chem. B* 114 (23), 7830–7843. *https://doi.org/10.1021/jp101759q*

33. Miyamoto, S., and Kollman, P. A. (1992) Settle: An Analytical Version of the SHAKE and RATTLE Algorithm for Rigid Water Models, *J. Comput. Chem.*13 (8), 952–962. https://doi.org/10.1002/jcc.540130805

34. Manglik, A., Kruse, A. C., Kobilka, T. S., Thian, F. S., Mathiesen, J. M., Sunahara, R. K., Pardo, L., Weis, W. I., Kobilka, B. K., and Granier, S. (2012) Crystal Structure of the Mu-Opioid Receptor Bound to a Morphinan Antagonist. *https://doi.org/10.2210/pdb4dkl/pdb*

35. Roe, D. R., and Cheatham, T. E. (2013) PTRAJ and CPPTRAJ: Software for Processing and Analysis of Molecular Dynamics Trajectory Data, *J. Chem.Theory Computat.* 9 (7), 3084–3095. *https://doi.org/10.1021/ct400341p*

36. Ricarte, A., Dalton, J. A. R., and Giraldo, J. (2021) Structural Assessment of Agonist Efficacy in the μ-Opioid Receptor: Morphine and Fentanyl Elicit Different Activation Patterns, *J. Chem. Inf. Model.* 61 (3), 1251–1274. *https://doi.org/10.1021/acs.jcim.0c00890*

37. Cong, X., Campomanes, P., Kless, A., Schapitz, I., Wagener, M., Koch, T., and Carloni, P. (2015) Structural Determinants for the Binding of Morphinan Agonists to the μ-Opioid Receptor, *PLOS ONE* 10 (8), e0135998. *https://doi.org/10.1371/journal.pone.0135998*

38. Lipiński, P. F. J., Jarończyk, M., Dobrowolski, J. Cz., and Sadlej, J. (2019) Molecular Dynamics of Fentanyl Bound to μ-Opioid Receptor, *J. Mol. Model.* 25 (5). https://doi.org/10.1007/s00894-019-3999-2.

39. Gimpl, G. (2016) Interaction of G Protein Coupled Receptors and Cholesterol, *Chem. Phys.Lipids* 199, 61–73. *https://doi.org/10.1016/j.chemphyslip.2016.04.006*

40. Vukojevic, V., Ming, Y., D'Addario, C., Hansen, M., Langel, Ü., Schulz, R., Johansson, B., Rigler, R., and Terenius, L. (2008) μ-Opioid Receptor Activation in Live Cells, *FASEB J.* 22 (10), 3537–3548. *https://doi.org/10.1096/fj.08-108894*

41. Eberhardt, J., Santos-Martins, D., Tillack, A. F., and Forli, S. (2021) AutoDock Vina 1.2.0: New Docking Methods, Expanded Force Field, and Python Bindings, *J. Chem. Inf. Model.* 61 (8), 3891–3898 *https://doi.org/10.1021/acs.jcim.1c00203*

42. Trott, O., and Olson, A. J. (2009) AutoDock Vina: Improving the Speed and Accuracy of Docking with a New Scoring Function, Efficient Optimization, and Multithreading. *J. Comput. Chem.* 31 (2), NA-NA. *https://doi.org/10.1002/jcc.21334*

43. Vanommeslaeghe, and K., MacKerell, A. D. (2012) Automation of the CHARMM General Force Field (CGenFF) I: Bond Perception and Atom Typing, *J. Chem. Inf. Model.* 52 (12), 3144–3154. *https://doi.org/10.1021/ci300363c*

44. Vanommeslaeghe, K., Raman, E. P., and MacKerell, A. D. (2012) Automation of the CHARMM General Force Field (CGenFF) II: Assignment of Bonded Parameters and Partial Atomic Charges, *J. Chem. Inf. Model.* 52 (12), 3155–3168. *https://doi.org/10.1021/ci3003649*

45. Vanommeslaeghe, K., Hatcher, E., Acharya, C., Kundu, S., Zhong, S., Shim, J., Darian, E., Guvench, O., Lopes, P., Vorobyov, I., and Mackerell, A. D. (2010) CHARMM General Force Field: A Force Field for Drug-like Molecules Compatible with the CHARMM All-Atom Additive Biological Force Fields, *J. Comput. Chem.* 31 (4), 671–690. *https://doi.org/10.1002/jcc.21367*

46. Humphrey, W., Dalke, A., and Schulten, K. (1996) VMD: Visual Molecular Dynamics, *J. Mol. Graph.* 14 (1), 33–38. *https://doi.org/10.1016/0263-7855(96)00018-5*

47. Mayne, C. G., Saam, J., Schulten, K., Tajkhorshid, E., and Gumbart, J. C. (2013) Rapid Parameterization of Small Molecules Using the Force Field Toolkit, *J. Comput. Chem.* 34 (32), 2757–2770. *https://doi.org/10.1002/jcc.23422*

ABOUT THE STUDENT AUTHORS

Allison Barkdull is a senior undergraduate at the University of Florida studying biomedical engineering with a minor in physics. Lexin Chen is a chemistry Ph.D. student at the University of Florida. Her research is on building algorithms to analyze the molecular similarity of large datasets with applications to drug discovery. Akash Mathavan is a fourth year M.D. candidate at the University of Florida College of Medicine pursuing a career in internal medicine.

PRESS SUMMARY

The mu-opioid receptor is the primary target for pain-modulating drugs. However, existing opiate drugs have detrimental side effects such as addiction and respiratory depression. Molecular dynamics simulations allow the motion of the mu-opioid receptor to be studied with atomistic resolution. However, because the mu-opioid receptor is enclosed within the lipid bilayer, molecular dynamics simulations typically require the simulation of lipid molecules as well as the receptor, which requires a large amount of computational resources. This study proposes and evaluates an alternative method to simulate the mu-opioid receptor by adding restraints on the transmembrane regions of the protein to mimic the viscosity of the lipid bilayer without explicitly simulating lipid molecules. The proposed model allows the dynamics of the mu-opioid receptor to be simulated 49% faster than a model that involves explicitly simulated lipid molecules. This has the potential to speed up studies of mu-opioid receptor motion, aiding in discovering new opioid drugs.

SUPPLEMENTAL INFORMATION

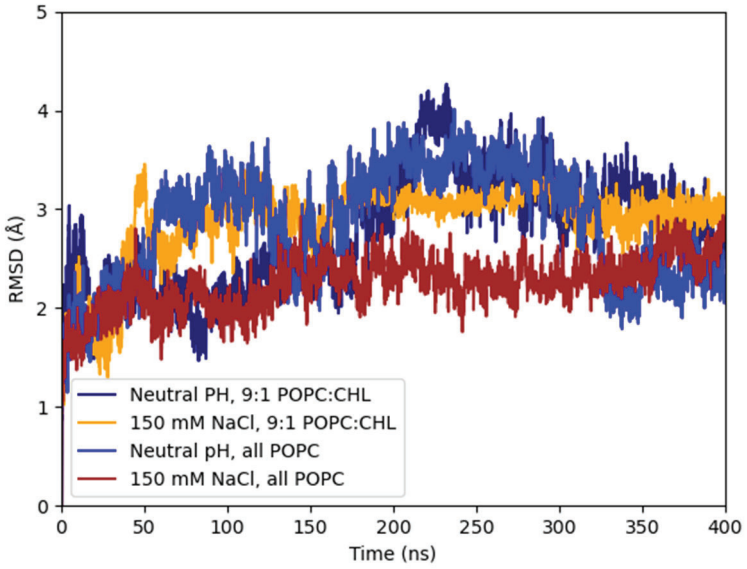

Supplemental Figure 1. The RMSD of MOR in an explicitly modeled lipid bilayer with either a membrane of either 100% POPC or 10% cholesterol and 90% POPC.